INSTITUTE OF PHYSICS PUBLISHING and INTERNATIONAL ATOMIC ENERGY AGENCY NUCLEAR FUSION

Nucl. Fusion **46** (2006) S888–S897 doi:10.1088/0029-5515/46/10/S04

Explanation of the JET $n = 0$ chirping mode

H.L. Berk[1], C.J. Boswell[2], D. Borba[3,4], A.C.A. Figueiredo[3], T. Johnson[5], M.F.F. Nave[3], S.D. Pinches[6], S.E. Sharapov[7] and JET EFDA contributors[8]

[1] Institute for Fusion Studies, University of Texas, Austin, TX, 78712, USA
[2] Plasma Science and Fusion Center, MIT, Cambridge, MA 02139, USA
[3] Centro de Fusão Nuclear, Associação EURATOM/IST, Instituto Superior Técnico, Av Rovisco Pais, 1049-001 Lisboa, Portugal
[4] EFDA Close Support Unit, Culham Science Centre, OX14 3DB, UK
[5] Alfvén Laboratory, KTH, Euratom-VR Association, Sweden
[6] Max-Planck Institute for Plasma Physics, EURATOM Association, Boltzmannstrasse 2, D-85748 Garching, Germany
[7] Euratom/UKAEA Fusion Association, Culham Science Centre, Abingdon, Oxon, OX14 3DB, UK

E-mail: hberk@mail.utexas.edu

Received 21 December 2005, accepted for publication 3 July 2006
Published 18 September 2006
Online at stacks.iop.org/NF/46/S888

Abstract
Persistent rapid up and down frequency chirping modes with a toroidal mode number of zero ($n = 0$) are observed in the JET tokamak when energetic ions, in the range of several hundred keV, are created by high field side ion cyclotron resonance frequency heating. Fokker–Planck calculations demonstrate that the heating method enables the formation of an energetically inverted ion distribution which supplies the free energy for the ions to excite a mode related to the geodesic acoustic mode. The large frequency shifts of this mode are attributed to the formation of phase space structures whose frequencies, which are locked to an ion orbit bounce resonance frequency, are forced to continually shift so that energetic particle energy can be released to counterbalance the energy dissipation present in the background plasma.

PACS numbers: 52.35.Mw, 52.35.Sb, 52.40.Mj

(Some figures in this article are in colour only in the electronic version)

1. Introduction

Future burning plasma experiments, such as ITER, will be dealing with a plasma consisting of a core thermal component characterized by some base temperature (e.g. 15–25 keV in ITER), an energetic alpha particle component with much higher energies and energetic ions produced by neutral beam injection (NBI) and/or by ion cyclotron (ICRF) heating. Such plasmas often give rise to nonlinear phenomena that are based on both MHD fluid properties and intrinsic kinetic particle properties. In this paper we explain the origin of an unusual set of data observed in JET (first noted by Heeter 1999) that shows persistent, high clarity, up and down frequency chirping modes with $n = 0$ (n is the toroidal mode number) (Figueiredo and Nave 2005, Boswell *et al* 2006). We infer that these oscillations are due to the combined effects of MHD fluid behaviour that is related to the geodesic acoustic mode (GAM) (Winsor *et al* 1968) and zonal flow (see Diamond *et al* 2005, Conway *et al* 2005, Scott 2005 and references therein) and the response arising from the kinetic resonant interaction of the GAM with the energetic particle component. These chirping modes are experimentally established only when high field side (HFS) ICRF heating is applied (i.e. the ICRF resonance layer is on the HFS of the magnetic axis of the tokamak) and if the power applied by NBI is not too large (typically <5 MW). Most of these frequency chirping modes have been observed in discharges with a reversed magnetic shear as evidenced by the existence of Alfvén cascades (ACs) (Sharapov *et al* 2001, Berk *et al* 2001), but they have also been observed in discharges with steady frequency toroidal Alfvén eigenmodes (TAEs) and no ACs, suggesting that these modes can be established in plasmas with flat or monotonic q-profiles.

[8] See the appendix of Pamela J *et al* 2004 *Proc. 20th Int. Conf. on Fusion Energy (Vilamoura, 2004)* (Vienna: IAEA).

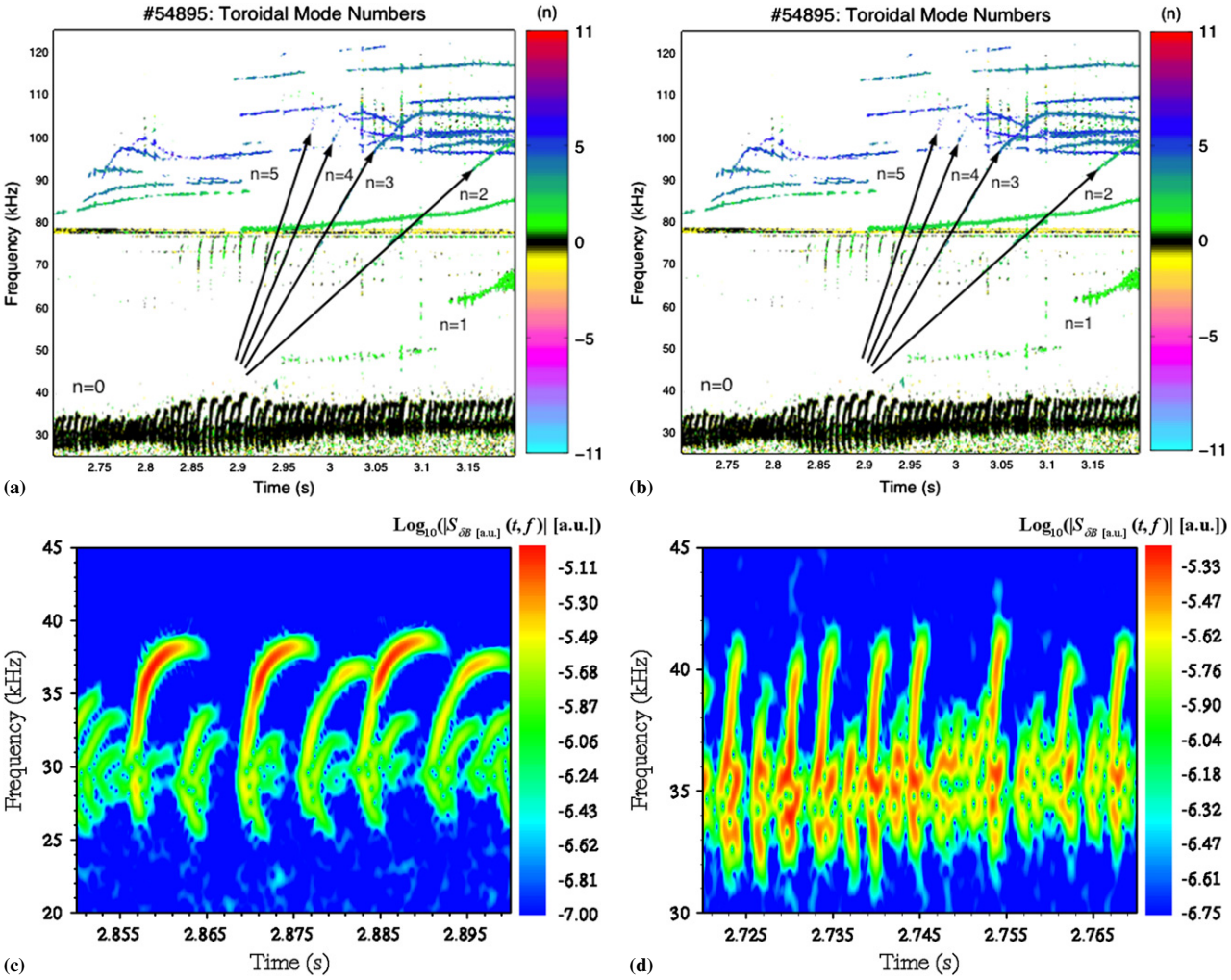

Figure 1. Frequencies for various toroidal n-numbers picked up by magnetic Mirnov signals in JET discharges: (a) #54895 and (b) #54899. Zooms of the frequency of the $n = 0$ mode are shown in (c) and (d) for discharges #54895 and #54899, respectively. In the legends of (c) and (d) $S_{\delta B}(t, f)$ is the short-time Fourier transform of δB with arbitrary units for δB and S.

Among the issues addressed here are the identification and mechanism of excitation of the basic plasma mode being observed. We present the evidence for why this mode is related to the GAM and explain why the source of the frequency chirping must come from an instability drive that is due to the inversion of the energetic ion population, where $\partial F(E, \mu, P_\phi)/\partial E|_{\mu,P_\phi} > 0$ (in this experiment E, μ and P_ϕ are, respectively, the energy, magnetic moment and canonical angular momentum of hydrogen particles generated by ICRF minority heating). Because this phenomenon arises for an $n = 0$ mode, these low frequency excitations (relative to the ICRF frequency) effectively cause nonlinear particle motion in one dimension as μ and P_φ are conserved. As a result the ultimate theoretical understanding of this phenomenon may be easier to achieve than other related chirping excitations, such as those observed in the excitation of fishbones (McGuire *et al* 1983) and frequency sweeping modes in the TAE-frequency range (Heidbrink 1994, Shinohara *et al* 2001, Pinches *et al* 2004) in two component burning-plasma-related experiments. Hence, even though this specific $n = 0$ mode observed in JET may or may not occur in a burning plasma experiment, its complete description will allow deep insight into the nature of frequency chirping–fluid flow interactions that will certainly be relevant to burning plasma experiments.

2. Experimental data

In figure 1 we show two specific cases (JET discharges #54895 and #54899) where $n = 0$ chirping oscillations have been observed. In figure 1(a) we see the usual spectra of Alfvénic activity (both ACs and TAEs) at about 100 kHz for toroidal n-numbers 1–5 that are detected by edge Mirnov coils. In this case there is a general slow upsweep of the AC frequency to the TAE range of frequency, indicating that a shear reversed configuration is present (Sharapov *et al* 2001, Berk *et al* 2001). In JET discharges #54899 a similar spectrum of Alfvénic activity is seen in the 100 kHz range in figure 1(b) but with the mode frequencies remaining rather constant in time. These are TAE excitations, and the lack of ACs indicates that the q-profile is flat or monotonic for this discharge. However, both discharges exhibit rapid frequency chirping modes around the 30 kHz range and the chirping pulses are constantly repeating. These two discharges were characterized by HFS ICRF heating (∼5 MW) and the chirping persisted the entire time ICRF

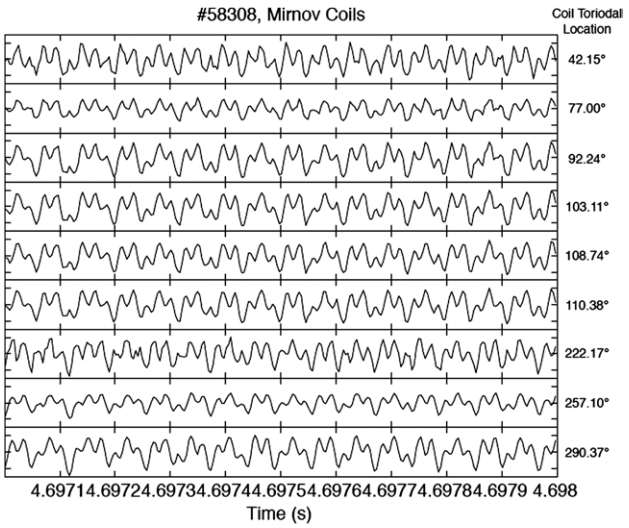

Figure 2. The low frequency response magnetic signal as a function of time, picked up by Mirnov coils situated at various toroidal angular positions all at the outer poloidal mid-plane for discharge #58308.

heating was applied. Figures 1(*c*) and (*d*) are blow-ups of the chirping spectral regions. The spectrograms appearing there were obtained by applying a short time Fourier transform technique (Claasen and Mecklenbräuker 1980). We see that for the reversed shear discharge (#54895) the frequency is initially at ∼30 kHz and in 2–3 ms sweeps up and down in frequency to about 25 kHz and 35 kHz, respectively. The upsweep component continues to sweep even longer, for up to 5 ms, with the upsweep frequency reaching 38 kHz. The chirping cycle repeats itself in 7–8 ms. Similar behaviour is seen for the non-reversed case shown in figure 1(*d*). The initial frequency is ∼35 kHz, and there is an up and down frequency chirp to 42 and 31 kHz, respectively, that takes place within 2 ms and the chirping cycle repeats itself in 3 ms. In all cases where these oscillations have been observed, the HFS ICRF heating produced proton tails of several hundred keV. These oscillations have not been seen with low field side ICRF heating and typically the oscillations are quenched by the application of more than 5 MW of NBI heating or the termination of the ICRF heating. In the various experiments the initial frequencies typically occur between 20 and 60 kHz. They simultaneously chirp upwards in frequency by as much as 40% and downwards in frequency by as much as 25% of the initial frequency.

Mirnov coils which determine their frequency and the toroidal mode number pick up these modes. Figure 2 displays the signals from Mirnov coils located at different values of toroidal angle on the outboard side of the tokamak. These signals show the $n = 0$ structure from discharge #58308. The time correlation of all the signals is readily apparent.

Additional properties of the $n = 0$ mode arise from examining the reflectometer signals, when the reflectometer is operated in an 'interferometer' mode (Sharapov *et al* 2004), and from the signals observed on the soft x-ray detectors installed in a horizontal port viewing a vertical plane 15.6° off the major radius. The soft x-ray signals indicate that the modes are localized near the plasma core by means of cross-correlation analysis between the signals from the x-ray detectors and the signal from a Mirnov coil, which of course implies that the modes have a significant magnetic component. The strongest diode signals are those whose view had a tangent to the magnetic flux surface at $r/a = 0.15$ and they exhibited correlation with the Mirnov coil signal at the same frequencies as the $n = 0$ mode. For example, the correlation for discharge #56945 is shown in figure 3(*b*). The bottom plot shows the raw signal from the Mirnov coil. In the shaded time interval, the Fourier transform of this signal is taken and the result is shown in the plot above the raw signal. We see, in the caption above that of the raw signal, that the largest spectral power signals lie in the range from 26 to 40 kHz, corresponding to the frequency spread of the observed chirping modes. Coincident with this frequency range is the cross correlation amplitude of the Mirnov signal with the line of sight soft x-ray signal of the amplitude and phase, as seen in the top two plots. We clearly see that the frequency spectrum of the x-ray signal, that arises from a peaked internal excitation, correlates closely with the magnetic $n = 0$ signal being picked up by the edge Mirnov coils.

Figures 4(*a*) and (*b*) show the oscillations of the $n = 0$ chirping modes for discharges #54895 and #54899 over an extended period time. As indicated in the lower curves of figures 4(*a*) and (*b*), the ICRF power is turned on from the zero power level on the left-hand side of the curve and reaches a maximum of 5 MW for discharge #54895 and 7.87 MW at 2.5 s for discharge #54899. The central curves (the smoothest curves) are plotted in a linearly normalized scale of $T_e^{1/2}(r/a = 0.15)$ (in figure 4(*a*) $T_e^{1/2}(r/a = 0.15)$ starts at $(0.85\,\mathrm{keV})^{1/2}$ at 2.0 s and reaches $(3.35\,\mathrm{keV})^{1/2}$ at 3.0 s, while in figure 4(*b*) $T_e^{1/2}(r/a = 0.15)$ starts at $(1.05\,\mathrm{keV})^{1/2}$ and reaches $(4.02\,\mathrm{keV})^{1/2}$ at 3.5 s). A substantial change in the initiation frequency is observed in both discharges as the electron temperature changes and there is a very good correlation of the initiation frequency with the time varying electron temperature.

The data shown in figure 5 indicates that neutral beams do not encourage the conditions for chirping. This figure shows results from JET discharge #55317. Here the $n = 0$ mode is excited when 8.4 MW HFS ICRF heating together with 4.0 MW of neutral beam heating is applied. In the case the $n = 0$ exists for a large fraction of the discharge period at a nearly constant frequency, rather than the nearly continual chirping. Later in time the NBI power is increased to 6.8 MW. We see in figure 5 that the increased neutral beam heating appears to first cause an upshift of the frequency of the $n = 0$ mode, but then the $n = 0$ oscillations abruptly terminate.

3. Interpretation of data

3.1. Linear wave theory

The experimental data shown in figures 4(*a*) and (*b*) indicate that the basic mode frequency scales as $T_e^{1/2}$. This scaling suggests that the GAM is relevant to the description of the $n = 0$ chirping modes. The continuum GAM mode was predicted by Winsor *et al* (1968) to arise in a tokamak as an electrostatic $n = 0$ mode with the approximate dispersion relation given in the large aspect ratio and low beta (β) limit by

$$\omega^2 = \frac{\gamma p}{\rho R^2}\left(2 + \frac{1}{q^2}\right), \qquad (1)$$

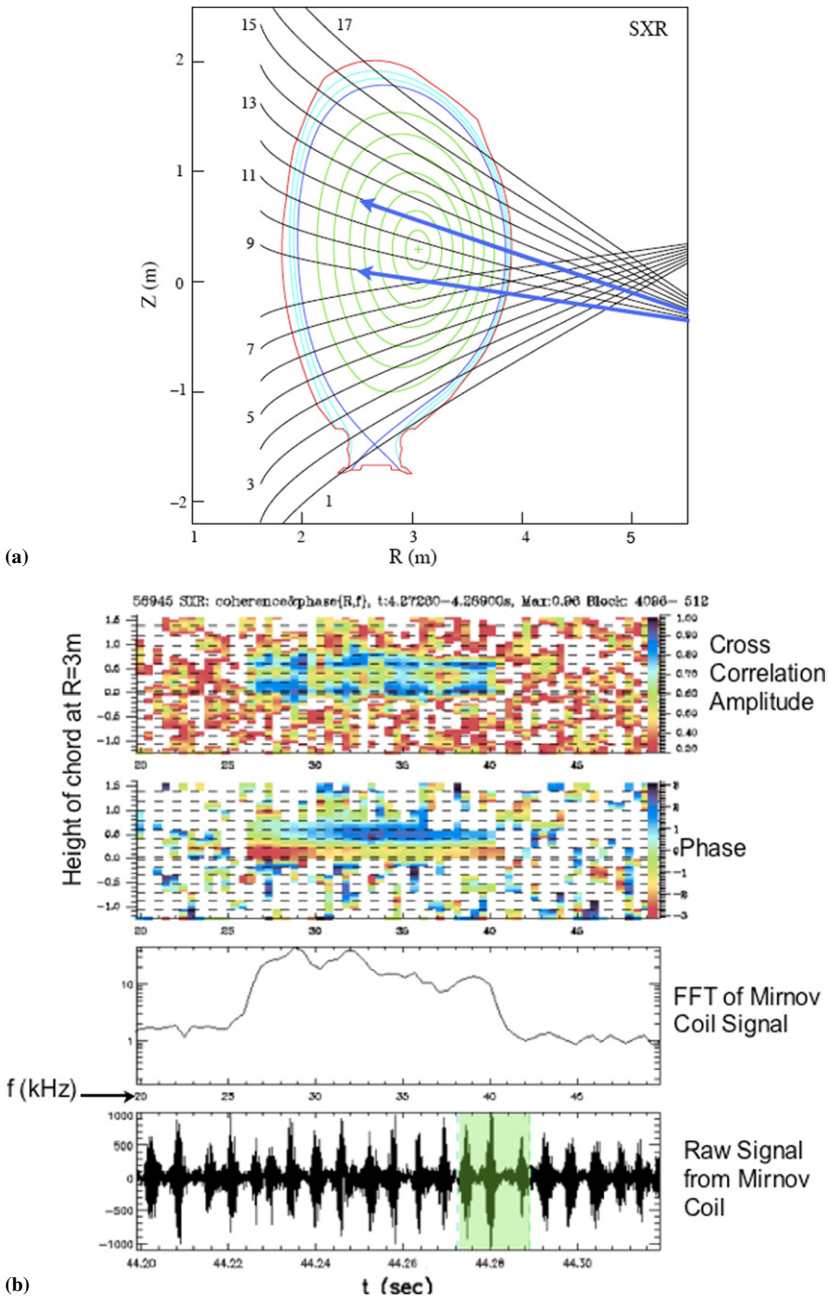

Figure 3. Soft x-ray signal measurements for discharge #55945. The line of sight positions are shown in (*a*). In (*b*), in the bottom panel, is seen the raw signal on the Mirnov coil as a function of time. The panel just above the Fourier transform of the shaded region shows that the highest intensity signals occur between the frequencies 27–40 kHz. The soft x-ray and Mirnov signals are found to correlate both in amplitude and phase as a function of frequency as is shown in the top two panels.

where γ is the adiabatic constant, p is the plasma pressure, ρ is the mass density and R is the major radius of the tokamak. When $T_e \gg T_i$, as is the case for chirping modes being observed in JET, the observed scaling of the frequency with temperature is obtained, as then $p/\rho = T_e$. It can be shown, when $T_e \gg T_i$, that kinetic MHD theory produces an identical dispersion relation to equation (1) with $\gamma = 1$ (Mazur and Mikhajlovskij 1977, Lebedev *et al* 1996).

Recently, it has been noted that the GAM also arises for finite-n values, on magnetic field lines that close on themselves (Breizman *et al* 2005). However, topologically the $n = 0$ case is special. Whereas with finite n-values, electrostatic GAMs are localized to one surface at a particular rational q-value, the $n = 0$ GAM allows the excitation of a continuous packet of frequencies over an extended and continuous region of flux surfaces. If these frequencies can be locked together by either linear or nonlinear processes, a global mode can form. Such synchronization has been found in the study of the regulation of drift wave turbulence by zonal flow (Diamond *et al* 2005, Scott 2005), where the global structure of the GAM is attributed to the anisotropy of particle sources and turbulent fluxes. Other properties such as finite Larmor radius effects, and the modification of the plasma response from the dynamics of the energetic particles, may also allow a global

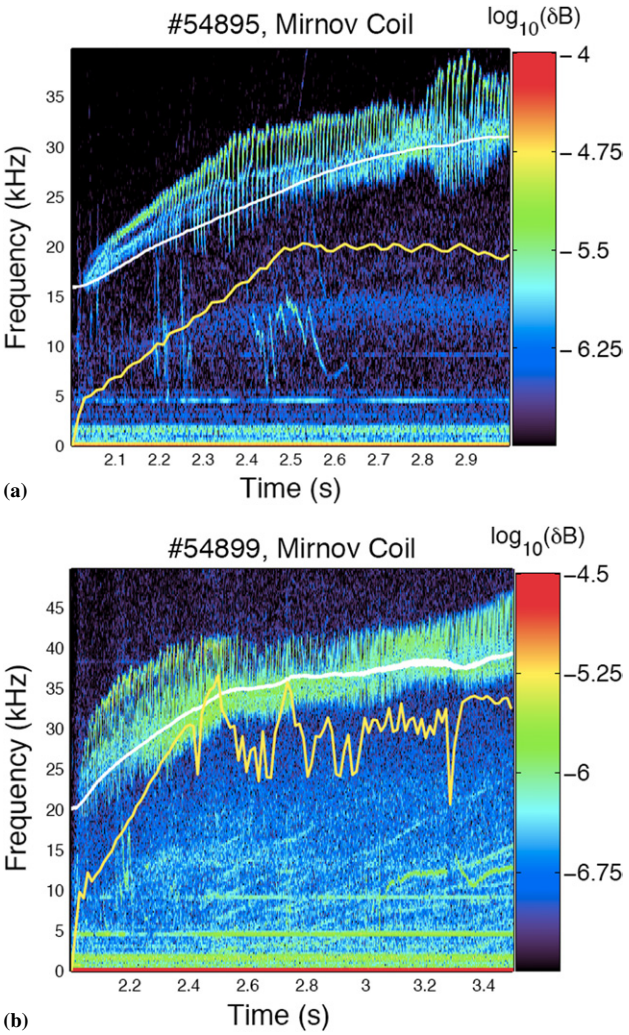

Figure 4. Plots of the frequency and square root of electron temperature (white curves in middle of mode oscillations) versus time for discharges (*a*) #54895 and (*b*) #54899 show the correlation between the mean frequency and the square root of electron temperature. The lowest curves show ICRF power applied.

mode to be established. In this work we point out another possible mechanism for establishing a radially extended GAM. We find that when the local GAM frequency has a maximum at a finite radial position, one then finds a global geodesic acoustic mode (GGAM) purely from MHD theory (Boswell *et al* 2006). It follows from equation (1) that finding such a maximum requires $\partial q/q\partial r = (q^2 + 1/2)\partial T_e/T_e\partial r$ (here assuming $T_e \gg T_i$). Thus, when shear reversal is present, the GAM frequency can have a maximum inside the shear reversal point. If $\partial T_e/T_e\partial r > 0$ near the axis, it is also possible to have an off-axis maximum for the GAM mode, although this possibility does not appear to be compatible with JET data that indicates that $\partial T_e/T_e\partial r$ is monotonically decreasing. The eigenmode structure of the GGAM is found to have a similarity to the GAM in the core of the mode, while the 'wings' of mode have a significant magnetic component. To make a comparison we first present an analytic description of the local GAM.

The local properties of the GAM are obtained by examining the following equations that have been derived for a continuum mode (Cheng and Chance 1986) on a magnetic

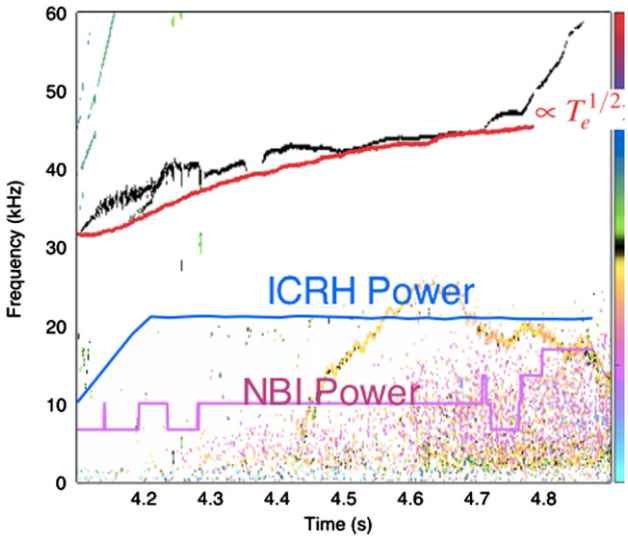

Figure 5. Plots of frequency, ICRH power and neutral beam power versus time for discharge #55317. The peak ICRH peak power is at 8.5 MW and the ICRH and NBI power plots are on a linear scale.

flux surface,

$$\rho\frac{\omega^2|\nabla\psi|^2}{B^2}Y + \frac{\partial}{J\partial\theta}\left(\frac{|\nabla\psi|^2}{B^2J}\frac{\partial Y}{\partial\theta}\right) + \gamma p\kappa_s Z = 0, \qquad (2)$$

$$\kappa_s Y + \left(\frac{\gamma p + B^2}{B^2}\right)Z + \frac{\gamma p}{\rho\omega^2 J}\frac{\partial}{\partial\theta}\left(\frac{1}{B^2J}\frac{\partial Z}{\partial\theta}\right) = 0. \qquad (3)$$

Here ψ is the poloidal magnetic flux surface, $p(\psi)$ is the equilibrium pressure, $\rho(\psi)$ is the equilibrium density, γ is the adiabatic index, the magnetic field is given by $\vec{B} = \nabla\phi \times \nabla\psi + q(\psi)\nabla\psi \times \nabla\theta$, the Jacobian is $J = (\nabla\psi \times \nabla\theta \cdot \nabla\phi)^{-1}$ with ϕ and θ toroidal and poloidal magnetic coordinates, the geodesic curvature is proportional to $\kappa_s \equiv 2\vec{\kappa} \cdot (\vec{B} \times \nabla\psi/B^2)$ with $\vec{\kappa}$ the magnetic curvature and the ideal MHD displacement is denoted by $\vec{\xi}$. In addition we have defined

$$Y(\theta) = \vec{\xi} \cdot (\vec{B} \times \nabla\psi/|\nabla\psi|^2)\exp[\mathrm{in}(\phi - q(\psi)\theta)]$$

$$Z(\theta) = \nabla \cdot \vec{\xi}\exp[\mathrm{in}(\phi - q(\psi)\theta)].$$

In this study we restrict ourselves to $n = 0$.

We now search for a low frequency mode. Note in equation (2) that a balance between the first and second Y terms produces $\omega^2 \approx k_\parallel^2 V_A^2$. To avoid such a solution we must take $Y(\theta)$ nearly constant in θ and assume that any deviation from this constant is small and vanishes as β (the ratio of kinetic to magnetic pressures) vanishes. We can choose the constant to be unity, so that with $Y(\theta) = 1 + \delta Y(\theta)$ and with $\delta Y(\theta) = 1$, equations (2) and (3) become

$$\frac{\partial}{\partial\theta}\left(\frac{|\nabla\psi|^2}{B^2J}\frac{\partial\delta Y}{\partial\theta}\right) = -J\gamma p\kappa_s Z - \rho\frac{\omega^2 J|\nabla\psi|^2}{B^2}, \qquad (4)$$

$$Z + \frac{\gamma p}{\rho\omega^2 J}\frac{\partial}{\partial\theta}\left(\frac{1}{B^2J}\frac{\partial Z}{\partial\theta}\right) = -\kappa_s. \qquad (5)$$

Now we integrate equation (4) in θ and *use* the periodicity of $Y(\theta)$ and $\mathrm{d}Y(\theta)/\mathrm{d}\theta$ over the 2π period $\theta = 2\pi$ to find

$$\int_{-\pi}^{\pi}\mathrm{d}\theta J\left(\gamma p\kappa_s Z + \rho\frac{\omega^2|\nabla\psi|^2}{B^2}\right) = 0. \qquad (6)$$

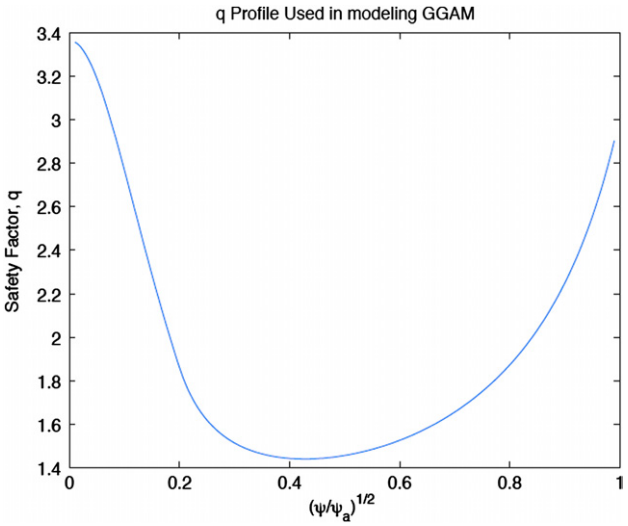

Figure 6. Plot of q-profile versus normalized square root of poloidal flux for model calculation.

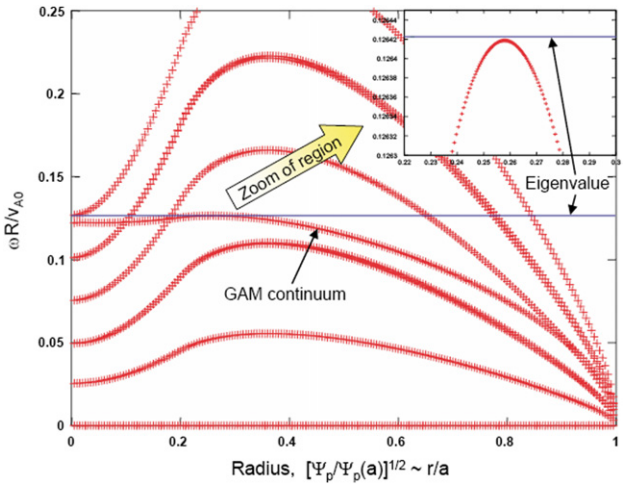

Figure 7. Frequency of $n = 0$ continuum modes found in model calculation.

We now need to solve for Z in equation (5) and substitute the solution into equation (6) to obtain the eigenmode for the system. The solution is particularly simple in the high aspect ratio, circular cross section limits, to which we now restrict our discussion. We find $J = r/B_\theta, \vec{\kappa} = (-\hat{r}\cos\theta + \hat{\theta}\sin\theta)/R$, and $\kappa_s = 2\sin\theta B_\theta/B$. Note that in this limit all quantities except the specific trigonometric functions are surface independent. We then find that the solution to equation (5) is

$$Z(\theta) = \frac{-2\sin\theta B_\theta/B}{1-(\gamma p/(\rho\omega^2(rB/B_\theta)^2))} = \frac{-2\sin\theta B_\theta/B}{1-(\gamma p/(\rho\omega^2 q^2 R^2))}. \tag{7}$$

Then substituting this expression and the relation $\kappa_s = 2\sin\theta B_\theta/B$ into equation (6), we find that the eigenfrequency given by equation (1) emerges. Inserting this value for ω^2 in equation (7) then yields

$$Z(\theta)/Y(\theta) \approx -\sin\theta\frac{B_\theta}{B}(2+1/q^2). \tag{8}$$

The MHD normal mode analysis code CASTOR (Kerner *et al* 1998) was used to study whether spatially extended GAM related excitations can be obtained from MHD theory. We chose a model reversed shear equilibrium with circular cross section with the q-profile shown in figure 6. The density is taken constant and the temperature varies as $T = T_0(1-r^2/a^2)$ where r is the minor radius and a the plasma edge. In addition $c_s/V_A = 0.066$ is the on-axis value of ratio of sound to Alfvén speeds. The continuum $n = 0$ GAM modes (characterized by a large $m = 0$ component) for this equilibrium profile are shown in figure 7. Most of the curves plotted are the continuum acoustic modes which do not have large $n = 0$ excitations. The flattish curve with the weak maximum is the curve for the GAM continuum frequencies. Only this continuum mode has a large $m = 0$ excitation. We also find a global eigenmode whose eigenfrequency lies just above the maximum frequency of the GAM continuum. We call this mode a GGAM. In figure 7 the horizontal line that lies barely above the GAM frequencies marks the frequency found for the GGAM. This is shown in the zoom blow-up inserted in figure 7. The global eigenmode structure is shown in figure 8 for the three components of the vector potential $\vec{A} = \vec{\xi}\times\vec{B}$, with $A_1 = \vec{A}\cdot\nabla\psi/|\nabla\psi|$, $A_2 = \vec{A}\cdot\nabla\theta/|\nabla\theta|$ and $A_3 = \vec{A}\cdot\nabla\phi/|\nabla\phi|$. We see that A_1 is highly localized, but A_2 and A_3 are spatially extended in space. Somewhat surprisingly, these eigenfunctions show that the $m = 2$ mode dominates the $m = 1$ mode, which we expected to be more important on the basis of the continuum mode theory. However, in order to better compare with the global eigenmode predictions obtained with CASTOR with the predictions of the GAM we construct from $\vec{A} = \vec{\xi}\times\vec{B}$ the functions $Y(\theta) = \vec{\xi}\cdot(\vec{B}\times\nabla\psi/|\nabla\psi|^2)$ and $Z(\theta) = \nabla\cdot\vec{\xi}$. These eigenfunctions are shown in figure 9. Now we observe that Y and Z are both localized in space, just in the region of the maximum frequency of the GAM mode, with Y dominantly an $m = 0$ mode while Z is primarily an $m = 1$ mode which are the expected dominant components on the basis of the local GAM theory. The ratio of $Z(\theta)/Y(\theta)$ at the maximum radial position of these eigenfunctions agrees to within 30% of the value predicted by the local GAM theory given by equation (7). In addition we plot in figure 9 one of the components of the perturbed magnetic field perpendicular to the equilibrium field, $\delta B^g = \delta\vec{B}\cdot\vec{b}\times\nabla\psi/|\nabla\psi|$. We see that unlike Y and Z, which are spatially localized, the perturbed magnetic field is dominated by the $m = 2$ component and has a tail that extends to the plasma edge. Thus, these numerical results from CASTOR show that the GGAM mode is in the correct frequency range and its eigenstructure is compatible with the experimental observations that show that the $n = 0$ mode is generated in the core of the plasma but that magnetic perturbations reach out to the edge of the plasma where they are picked up by Mirnov coils.

3.2. *Instability drive*

The next issue to consider is why there should be a spontaneous excitation of $n = 0$ modes. The usual universal instability drive from energetic particles associated with the radial gradient of fast particles is not applicable since the $n = 0$ nature of the mode under consideration precludes coupling to this drive. Hence, in this case the source of instability

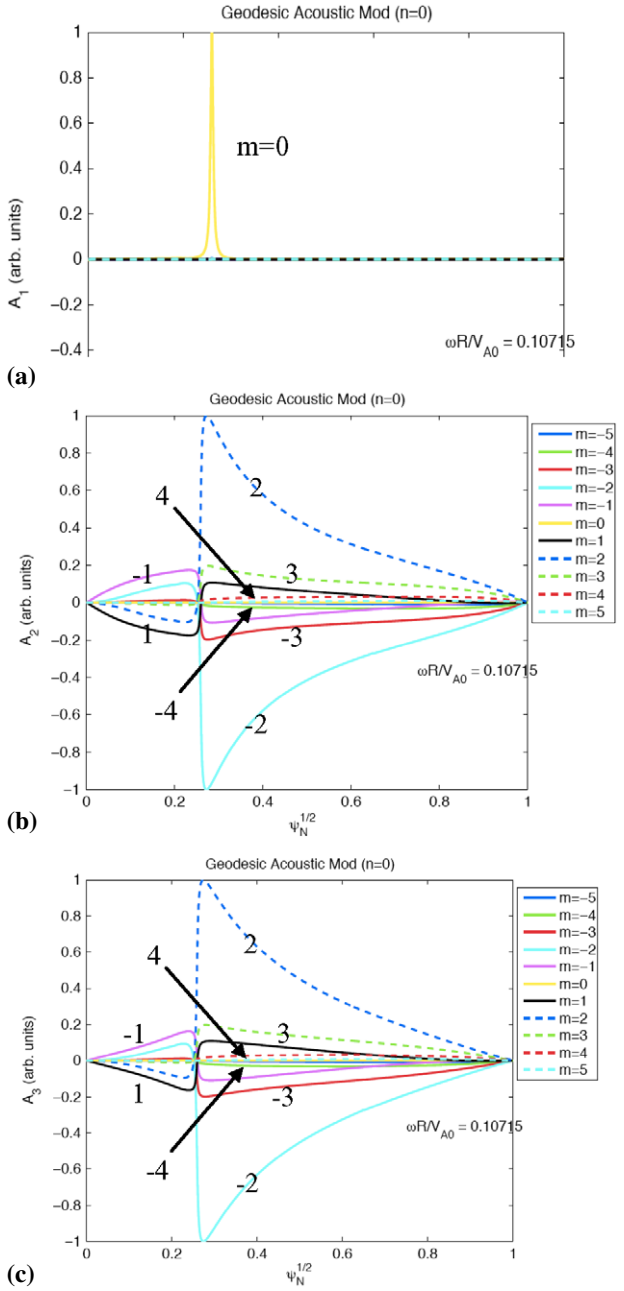

Figure 8. Plot of three components of the vector potential eigenfunction found from the CASTOR code.

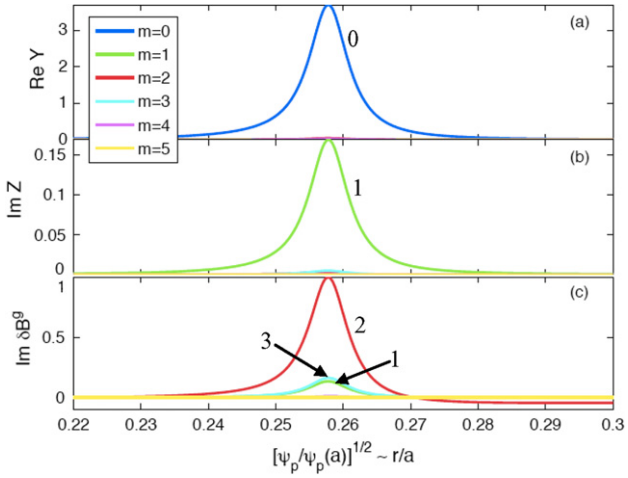

Figure 9. Plot of the eigenfunction of the CASTOR code, illustrating the spatial localization of the functions $\vec{\xi}\cdot(\vec{B}\times\nabla\psi/|\nabla\psi|^2)$ in (*a*) and $\nabla\cdot\vec{\xi}$ in (*b*). The perturbed magnetic field component shown in (*c*) is seen to have a tail that reaches out to the plasma edge.

must come from a group of particles whose distribution function, $F(E,\mu,P_\phi)$, has the energy inversion property $\partial F(E,\mu,P_\phi)/\partial E|_{\mu,P_\phi} > 0$. To determine whether such a drive is a property of the high-energy protons that are likely to be generated in this experiment, the Monte–Carlo SELFO code (Hellsten *et al* 2004) was used for determining the distribution function for HFS ICRF heated minority protons heating in a JET-like tokamak geometry. Previous studies have verified the ability of the SELFO code to model minority-heating scenario similarly to the one of interest, see e.g. (Mantsinen *et al* 2002).The results of the Monte–Carlo calculation indicate that the mean energy of the resonantly accelerated protons is ∼0.5 MeV. Most importantly, it was found that for the given magnetic moment and angular momentum, the mirror trapped energetic protons do indeed form a distribution function where $\partial F(E,\mu,P_\phi)/\partial E|_{\mu,P_\phi} > 0$. Similar energy inversion of the distribution function can be inferred from the so-called 'rabbit ear' distribution functions generated by Kerbel and McCoy (1985). This energy inversion is a property of the mirror trapped energetic protons whose turning points lie on the lower field side of the ICRF resonance. A plot of the inversion is shown in figure 10(*a*). This figure shows contours of constant distribution function as a function of energy (vertical coordinate) and magnetic moment (horizontal coordinate) at a fixed value of canonical momentum. The arrow shown in the figure covers the range in which the distribution is inverted. In contrast, the distribution function for low field side ICRF heating, as shown in figure 10(*b*), has a much smaller inversion region. This reduction in the phase space with low field side heating should then lead to a substantially smaller instability drive than the drive arising from HFS ICRF heating. Thus, these comparative figures indicate that spontaneous excitation of instability from an inverted distribution is much more likely to occur from HFS ICRF heating than from low field side ICRF heating.

3.3. Frequency sweeping

We attribute the pronounced frequency sweeping of the $n = 0$ modes to the formation of phase space structures, whose general nonlinear theory has developed in Terry *et al* (1990) and Berk *et al* (1997, 1998). It is required that the instantaneous experimental frequency be equal to an orbit resonance frequency, which in our case is the bounce orbit frequency of a magnetically trapped particle. The HAGIS code (Pinches *et al* 1998) was used to determine the bounce frequencies of particles with a fixed μ and P_ϕ and it was found that the experimental frequency range of the chirp (32–42 kHz) (the range of frequencies shown in figure 1(*d*)) for JET discharge #54899 corresponded to the bounce frequency range of particles whose energy varied from 220 to 260 keV, a region where the SELFO code indicates that the distribution was energy inverted. A plot of several of these orbits is shown in figure 11(*a*)

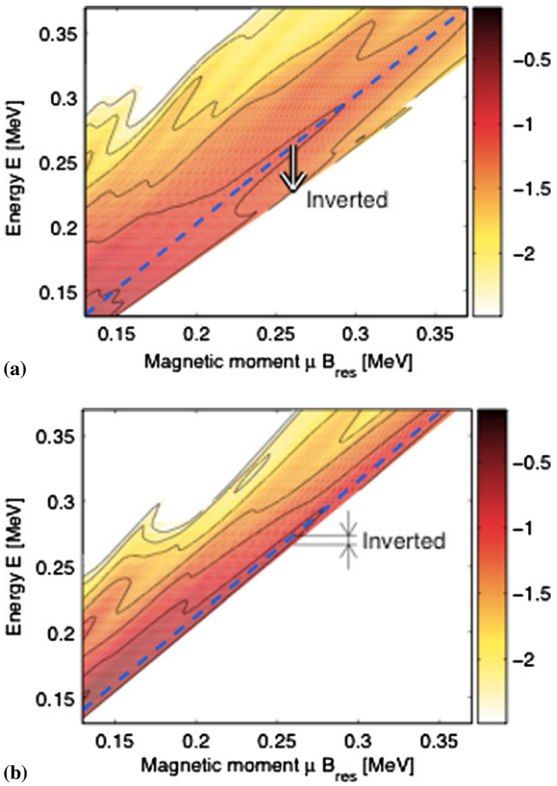

Figure 10. Greyscale and contours of the minority proton distribution function resulting from ICRF heating as found by the SELFO Monte Carlo code for variable energy and magnetic moment and fixed canonical angular momentum. The shading indicates the magnitude of $\log_{10} f$ of the distribution function with an arbitrary normalization of f. Neighbouring contours indicate a change by a factor of 2 of the distribution function. (*a*) is for the HFS heated distribution function ($B_0/B_{\rm res} = 0.9202$ where $B_{\rm res}$ is the magnetic field at the ICRF resonance and B_0 the magnetic field on axis) and the dashed curve on the figure represents (to a good approximation) the 'ridge' for which the distribution has a maximum as E changes on either side of the ridge. The vertical arrow spans the energy range in which the distribution is inverted, i.e. where $\partial F(E, \mu, P_\phi)/\partial E > 0$. The arrow lies in the region of phase space where the trapped particles' bounce frequency is comparable to the experimentally observed chirping frequencies. (*b*) is for the low field side heated distribution function where $B_0/B_{\rm res} = 1.0866$.

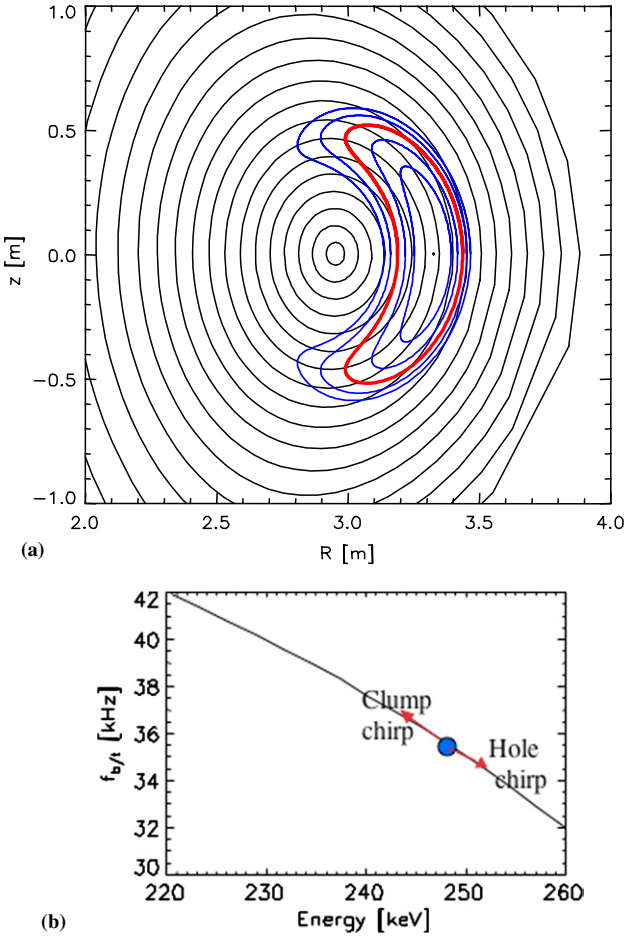

Figure 11. (*a*) Guiding center orbit trajectories found using the HAGIS code at fixed canonical toroidal angular momentum and magnetic moment. (*b*) Relation of the bounce frequency of particles versus the particle energy at fixed canonical toroidal angular momentum and magnetic moment.

and the functional dependence between bounce frequency and proton energy is shown in figure 11(*b*). The thickest trajectory in figure 11(*a*) corresponds to the orbit that is resonating with the onset frequency at 35.5 kHz corresponding to the linear frequency of a GGAM. Orbits with a larger energy, at fixed μ and P_ϕ, lie outside the thick trajectory, while orbits with a smaller energy at fixed μ and P_ϕ lie inside the thick trajectory. It should be noted that it is the nature of mirror confinement that trapped orbits possess a so-called effective negative-mass effect (Clarke and Kelley 1968) where higher (lower) energy particles correspond to lower (higher) bounce frequencies. Hence, with fixed μ and P_ϕ the lowest energy and the highest frequency reached by a particle corresponds to the bounce frequency of a deeply trapped particle and a particle whose banana tip is at the ICRF resonance point has a higher energy and lower bounce frequency than the particles that are resonant with the initiation frequency of the chirping $n = 0$ mode.

The changing mode frequency in the experiment is interpreted as a synchronism between the mode frequency and the resonance frequency as explained in Berk *et al* (1997, 1998). In the phase space region associated with a given mode frequency there are particles trapped in the fields of the wave. The distribution functions of these trapped particles are in the form of a clump (hole) where the wave trapped particle distribution has a larger (smaller) value than the ambient distribution. The clump (hole) cannot be stationary in time, as the structure needs to compensate for the power being absorbed by dissipation present in the background plasma. This forces the structure to move in phase space in a manner that extracts energy from the distribution function. Then the mode frequency synchronized with this structure shifts likewise. Hence, a clump (hole) must head to lower (higher) energy, and thus, because of the energy dependence of the bounce frequency of mirror-trapped particles, the frequency must increase (decrease). This description is compatible with the signals in figure 1 where the highest frequency signals are stagnating in time. They can be interpreted as clumps that have been convected in phase space to the deeply trapped mirror orbits of the tokamak. Having reached the maximum bounce frequency of the particles, there is no higher frequency

to shift to. Note that in this experiment the frequency increase (decrease), associated with the motion of clumps (holes), is of opposite sign to that which arises in most other reported chirping events, such as in the bump-on-tail instability (Berk *et al* 1997, 1998) or TAEs (Pinches *et al* 2004).

3.4. Non-chirping modes

Figure 5 shows an example of a sustained $n = 0$ mode excited without any pronounced rapid chirping when 8.5 MW of HFS ICRF heating and 4 MW of 80/120 keV MBI was applied. The energetic ∼0.5 MeV proton tails are, primarily, directly heating electrons, but the ion beams heat ions more strongly than electrons. As a result, in these experiments the ratio of T_i/T_e is expected be significantly larger than in the ICRF heating experiments without neutral beams. The increase in this ratio should enable an increased frequency of the GAM mode because for the MHD model we are using the frequency is proportional to $(T_e + T_i)^{1/2}$ (a kinetic based model (Lebedev *et al* 1996) predicts that the frequency is proportional to$(T_e + 7T_i/4)^{1/2}$). Thus, accounting for a finite T_i/T_e would increase the frequency of the theoretical curve and that should cause the correlation of experimental and theoretical frequencies to be closer to each other than we have indicated in figures 5 and 4(*a*) and (*b*). The most pronounced consequence of finite T_i/T_e is most strongly seen in figure 5 when the neutral beam power is increased to 6.8 MW. We then see in figure 5 an immediate increase in the frequency from 42 to 58 kHz, which we attribute to the increase in T_i, as the other parameters are nearly stationary during the time of the observation.

We also note that when NBI is imposed, additional dissipative processes arise that can prevent the GGAM from being spontaneously excited. Two additional mechanisms are apparent. These are the thermal ion Landau damping that arises from the increased ratio of T_i/T_e and the other is the resonance damping that arises from the neutral beams themselves which forms a monotonically decreasing slowing down distribution function as a function of energy for constant μ and P_ϕ. We suggest that these increased dissipative processes are the cause of the observed quenching of the spontaneous excitation of the GGAM that takes place following the imposition of too much power in the neutral beams. In figure 5 we see this quenching, but only after a time delay of ∼0.1 s during which the above-mentioned increase of the GGAM initiation frequency arises.

4. Summary and conclusion

The observation of the $n = 0$ chirping modes on JET has been attributed to the excitation of the GAM in plasmas where $T_e/T_i \gg 1$ and where minority species protons form high-energy tails from HFS ICRF heating. In such plasmas, the energetic tail primarily heats electrons and the deuterium ion temperature, which is not directly heated, remains low. We find that the starting mode frequency of fast chirping modes scales as the square root of the electron temperature. The only known modes that fit this scaling are the ion acoustic modes and the GAM. However, the properties of the ion acoustic mode are not particularly special for $n = 0$, and if the conditions are suitable in the plasma for their spontaneous excitation, then they should appear at many n-values. As only $n = 0$ chirping modes have been observed in this frequency range, it is difficult to attribute this observed mode to acoustic waves. This is because the GAM has very special properties that causes the predicted excitation to occur nearly always for $n = 0$. In principle, the GAM can appear at finite n-numbers but then they are constrained to be centred about a flux surface whose field lines close on themselves (i.e. field lines with a rational value of q). Thus, if such GAMs do arise at finite n-values, their mode frequency is very sensitive to equilibrium plasma parameters. This sensitivity has even been demonstrated in recently published JET data (Breizman *et al* 2005). But for a GAM, which has $n = 0$, the sensitivity to equilibrium parameters disappears as the GAM can be excited even without the side condition that the field line closes on itself. Then the GAM can be easily generated and even move continuously to neighbouring flux surfaces.

Our work shows that the edge magnetic signals picked up by Mirnov coils are synchronized to the internal modes that are measured from soft x-ray signals. The correlation of edge magnetic signals with an interior GAM excitation is somewhat of a surprise as the GAM is expected to be an electrostatic mode. However, the CASTOR MHD code shows that under suitable conditions (in the CASTOR calculation it is when GAM frequency has a local maximum as the flux surface varies) a global GAM mode can be established. The code then shows that the mode structure contains an interior 'core' where the plasma displacement is localized spatially with polarization properties similar to that of continuum mode theory. In addition a 'halo' arises which produces a magnetic perturbation that reaches the edge boundary.

Questions remain about how in general the spatial mode structure can be established. This work identified a MHD mechanism for establishing a global eigenmode under the special conditions mentioned above. This is one possibility but other mechanisms for establishing the GAM have been proposed (e.g. see Diamond *et al* 2005) and this issue still needs to be studied to achieve a more complete understanding of the linear mode structure.

The most important result found in the experiment is the observation that GAM modes produce continually rapid chirping. Previously the GAM had been associated with the regulation of fine scale fluid turbulence through a zonal flow. In the JET data presented here the geodesic mode has a different important function and that is to be the wave carrier that will support the formation of phase space structures when energetic particles form an inverted distribution function. Hence, we are seeing an intrinsic fluid effect associated with a zonal flow interacting with a highly kinetic effect, namely the formation of phase space structures.

Another feature of these $n = 0$ GAM modes deserves emphasis. Note that when this mode is excited, a particle still conserves its value of P_ϕ (since the mode is axi-symmetric) and μ (since the frequency is much less than the cyclotron frequency). This means the dynamics of an energetic particle is one-dimensional to a very high level of accuracy. This reduction of symmetry in a three-dimensional problem should allow precision analytic and numerical computations in future work and thereby lead to deeper insight into chirping phenomena due to the formation of phase space structures.

Chirping modes such as fishbones and TAE modes, where it is believed that it is the formation of phase space structures that lead to the rapid chirping, have been seen in a variety of Alfvénic instabilities. Chirping from these latter effects is likely to appear in burning plasma experiments when the alpha particle population can excite TAE modes.

Also note that figure 5 shows that under appropriate conditions the $n = 0$ mode appears at a nearly steady oscillation frequency rather than appearing as a repeated series of chirping modes. The observation of a relatively steady frequency supports the view that the global GAM established in the experiment is similar to other types of perturbative modes, such as the TAE, where the mode is supported by the plasma alone, independent of the energetic particles. This observation enables a self-consistent computer simulation of the experimentally observed chirping using the HAGIS code. As has been described in (Pinches *et al* 2004), this code uses an eigenmode and eigenfrequency (that can come from the CASTOR code) to supply the carrier mode, and HAGIS then uses equations derived from perturbation theory to determine the kinetic interactions of the carrier wave with energetic particles. This description can lead to the formation of phase space structures and the results will be described elsewhere.

It is interesting to consider whether the very pronounced kinetic effect generated by a GAM that is reported here can occur in a burning plasma experiment. The empirical evidence, which has thus far only shown that this mode occurs in plasmas where $T_e/T_i \gg 1$, indicates that chirping processes of the GAM are not likely to arise in a burning plasma where T_e and T_i are nearly equal. Nonetheless, supportive calculations still need to be performed to have confidence that this conclusion is correct. For example, we attributed the disappearance of the $n = 0$ mode to either the ion Landau damping that may arise as the ion temperature rises or the damping due to the presence of a neutral beam that has a slowing down distribution function. Indeed, since the GAM is a 'fast acoustic mode' (its phase velocity is larger than the sound speed by a factor $\sqrt{2q}$) there may not be substantial damping due to ion Landau damping when the internal q is relatively large ($q \sim 2$–3) . This is the case in some advanced burning plasma scenarios (Yarvorskij *et al* 2003). Thus, in some cases, the excitation of the $n = 0$ GAM may be possible in an advanced burning plasma experiment, where we expect $T_i/T_e \sim 1$ but with q larger than unity. Note that fusion born alpha particles always have degree of temperature anisotropy, which ranges from modest variations of $(T_{||} - T_\perp)/T_{||} \approx (r/R)^{3/2}$ in monotonic q-profiles (Stringer 1974) to unity in a magnetically shear reversed plasma of 'advanced' tokamaks (Yavorskij *et al* 2003). In conditions closer to the latter case, the alpha particles may have the free energy to spontaneously drive the chirping GAM mode. This instability only causes energy diffusion of alpha particles but no spatial diffusion as the canonical angular momentum is conserved and thus this instability does not lead to a parasitic loss of the energetic alpha particles. However, the repetitive GAM excitations are continually extracting energy from the alpha particles, and this energy is being transferred to the background plasma through the plasma dissipation that is giving rise to the chirping frequencies. This new channel for the absorption of alpha particle energy can complement the standard electron drag process as a method of transferring energy to the plasma core. As a consequence the population of energetic alpha particles would be lowered somewhat for a given amount of fusion energy production, thereby reducing the drive that can induce the parasitic loss of alpha particles due to Alfvénic instabilities.

A second application is to note that there is strong coupling of the GAM mode with zonal flows (Sugama and Watanabe 2006). If the GAM chirping is established by applying ICRH in burning plasmas, it may then be possible to have external control of the zonal flows and through this means have an external 'knob' to regulate turbulent diffusion.

Acknowledgments

We are indebted to Dr G.D. Conway for bringing to our attention the properties of the GAM. This work has been conducted under the European Fusion Development Agreement and was funded partly by US DoE contracts DE-FG02-99ER54563 and DE-FG02-04ER54742.

References

Berk H.L., Breizman B.N. and Petviashvili N.V. 1997 *Phys. Lett.* A **23** 213
Berk H.L., Breizman B.N. and Petviashvili N.V. 1998 *Phys. Lett.* A **238** 408 (erratum)
Berk H.L. *et al* 2001 *Phys. Rev. Lett.* **87** 185002
Boswell C.J. *et al* 2006 *Phys. Lett.* A **358** 154–8
Breizman B.N., Pekker M. and Sharapov S.E. 2005 *Phys. Plasmas* **11** 4939
Cheng C.Z. and Chance M.S. 1986 *Phys. Fluids* **29** 3695
Claasen T.A.C.M. and Mecklenbräuker W.F.G. 1980 *Philips J. Res.* **35** 372
Clarke J.F. and Kelley G.G. 1968 *Phys. Rev. Lett.* **21** 1041
Conway G.D. *et al* 2005 *Plasma Phys. Control. Fusion* **47** 1165
Diamond P.H., Itoh S.-I., Itoh K. and Hahm T. 2005 *Plasma Phys. Control. Fusion* **47** R35
Figueiredo A.C.A. and Nave M.F.F. 2005 *IEEE Trans. Plasma Sci.* **33** 468
Heeter R.F. 1999 Alfvén eigenmode and ion Bernstein wave studies for controlling fusion alpha particles PhD Thesis, Princeton University, USA
Heidbrink W.W. 1994 *Plasma Phys. Control. Fusion* **37** 4120
Hellsten T. *et al* 2004 *Nucl. Fusion* **44** 892
Kerbel G.D. and McCoy M.G. 1985 *Phys. Fluids* **28** 3629
Kerner W J *et al* 1998 *J. Comput. Phys.* **142** 271
Lebedev V.B., Yushmanov P.N. and Diamond P.H. 1996 *Phys. Plasmas* **3** 3023
Mantsinen M.J. *et al* 2002 *Phys. Rev. Lett.* **89** 115004
Mazur V.A. and Mikhajlovskij A.B. 1977 *Nucl. Fusion* **17** 193
McGuire K. *et al* 1983 *Phys. Rev. Lett.* **50** 891
Pinches S.D. *et al* 1998 *Comput. Phys. Commun.* **111** 133
Pinches S.D., Berk H.L., Gryazenvich M.P. and Sharapov S.E. 2004 *Plasma Phys. Control. Fusion* **46** S47
Scott B. 2005 *New J. Phys.* **7** 92
Sharapov S.E. *et al* 2001 *Phys. Lett.* A **289** 127
Sharapov S.E. *et al* 2004 *Phys. Rev. Lett.* **93** 165001
Shinohara K *et al* 2001 *Nucl. Fusion* **41** 603
Stringer T.E. 1974 *Plasma Phys.* **16** 651
Sugama H. and Watanabe T.H. 2006 *Phys. Plasmas* **13** 012501
Terry P.W., Diamond P.H. and Hahm T.S. 1990 *Phys. Fluids* B **2** 2048
Winsor N., Johnson J.L. and Dawson J.M. 1968 *Phys. Fluids* **11** 2448
Yavorskij V., Goloborod'ko V., Shoepf K., Sharapov S.E, Challis C.D., Reznik S. and Stork D. 2003 *Nucl. Fusion* **43** 1077